Coarsening and mechanics in the bubble model for wet foams

Khakalo, Kseniia; Baumgarten, Karsten; Tighe, Brian P.; Puisto, Antti

DOI
10.1103/PhysRevE.98.012607

Publication date
2018

Document Version
Final published version

Published in
Physical Review E

Citation (APA)
Khakalo, K., Baumgarten, K., Tighe, B. P., & Puisto, A. (2018). Coarsening and mechanics in the bubble model for wet foams. *Physical Review E*, *98*(1), Article 012607. https://doi.org/10.1103/PhysRevE.98.012607

Important note
To cite this publication, please use the final published version (if applicable).
Please check the document version above.

Coarsening and mechanics in the bubble model for wet foams

Kseniia Khakalo*
Aalto University, School Science, Laboratory of Applied Physics B.O.B 11100, FI-00076 AALTO, Finland

Karsten Baumgarten and Brian P. Tighe
Delft University of Technology, Process & Energy Laboratory, Leeghwaterstraat 39, 2628 CB Delft, The Netherlands

Antti Puisto
Aalto University, School Science, Laboratory of Applied Physics B.O.B 11100, FI-00076 AALTO, Finland

(Received 20 February 2018; published 19 July 2018)

Aqueous foams are an important model system that displays coarsening dynamics. Coarsening in dispersions and foams is well understood in the dilute and dry limits, where the gas fraction tends to zero and one, respectively. However, foams are known to undergo a jamming transition from a fluidlike to a solidlike state at an intermediate gas fraction ϕ_c. Much less is known about coarsening dynamics in wet foams near jamming, and the link to mechanical response, if any, remains poorly understood. Here we probe coarsening and mechanical response using numerical simulations of a variant of the Durian bubble model for wet foams. As in other coarsening systems we find a steady state scaling regime with an associated particle size distribution. We relate the time rate of evolution of the coarsening process to the wetness of the foam and identify a characteristic coarsening time that diverges approaching jamming. We further probe mechanical response of the system to strain while undergoing coarsening. There are two competing timescales, namely the coarsening time and the mechanical relaxation time. We relate these to the evolution of the elastic response and the mechanical structure.

DOI: 10.1103/PhysRevE.98.012607

I. INTRODUCTION

Aqueous foams are composed of gas bubbles dispersed in a continuous liquid phase. They are not thermodynamically stable, and the number and size of bubbles in a foam evolves in time. The three principal mechanisms driving temporal evolution are drainage, coalescence, and coarsening [1]. Drainage removes liquid between the bubbles via gravity. In addition, the liquid phase is exposed to evaporation. Coalescence, where bubbles join when thin films rupture between them, primarily takes place when the gas fraction is high. The final mechanism, namely coarsening, is the focus of the present work. Coarsening occurs when gas diffuses from smaller bubbles to larger ones due to the difference in their internal pressure [2].

Foams can be categorized by their gas volume fraction ϕ [1]. At low ϕ the foam is "wet" and bubbles mostly retain their spherical shape. In "dry" foams the gas fraction is high and bubbles assume polyhedral shapes, with neighboring bubbles separated by thin films of liquid. Coarsening is best understood in the extreme limits of perfectly dry foams ($\phi \to 1$) and "bubbly liquids" ($\phi \to 0$) [1]. However, geometric and mechanical properties of foams are known to undergo a sharp transition at an intermediate gas fraction ϕ_c ($\approx$0.84 in 2D and 0.64 in 3D) known as the jamming transition [3–9]. Close to but below ϕ_c, the system is a highly viscous liquid. Above ϕ_c, the average number of contacts per bubble exceeds a critical threshold and the system is solidlike, with an elastic storage modulus that exceeds its loss modulus on timescales that are short compared to coarsening-induced rearrangements. On either side of the transition, material properties are highly sensitive to the distance to jamming $\Delta\phi = \phi - \phi_c$. Surprisingly, while the significance of the jamming transition for structure and mechanics is well known, there is little understanding of the interplay between jamming and coarsening-driven dynamics. We expect such an interplay on two broad grounds. First, coarsening alters the bubble size distribution, which in turn influences ϕ_c. Hence the distance to jamming can vary dynamically, even when the gas fraction is constant. Second, coarsening introduces new timescales, and dynamical processes that are "slow" and "fast" compared to the evolution of the bubble size distribution are likely to proceed differently.

Our focus is on the so-called scaling state, where the bubble number density evolves in a unique self-similar fashion independent of the initial configuration [10] driven by the minimization of the total interfacial energy between the two phases [11]. This state is reached during prolonged coarsening in foams [1,12–14]. The system reaches the scaling state on some timescale τ_c that is characteristic of the coarsening dynamics. For longer times, the growth of bubbles reaches an asymptotic limit with the average radius following a power law:

$$\frac{\langle R\rangle}{\langle R_{\rm in}\rangle} \simeq \begin{cases} 1, & t \ll \tau_c, \\ (t/\tau_c)^{\alpha}, & t \gg \tau_c, \end{cases} \tag{1}$$

where $\langle R_{\rm in}\rangle$ is the average bubble radius at time $t = 0$. The exponent α can assume different values. In the dry limit, all

*kseniia.khakalo@aalto.fi

gas exchange occurs though the thin films separating bubbles; in bubbly liquids, by contrast, gas exchange is mediated by diffusion through the continuous fluid phase, with close analogies to ripening and domain growth. As a result of these distinct mechanisms, coarsening in the $\phi \to 1$ and $\phi \to 0$ limits is characterized by distinct exponents $\alpha = 1/2$ and $\alpha = 1/3$, respectively. Experiments have confirmed the existence of the scaling state and the respective exponents in the dry foam and bubbly liquid limits [2,12–14]. There is some numerical evidence that Eq. (1) is applicable for intermediate ϕ, with an effective exponent α that interpolates between the limiting cases [15]. To date, however, there have been no studies that systematically probe coarsening in the vicinity of the jamming point, nor is the ϕ dependence of the coarsening time τ_c known.

Here we model coarsening using a variant of the Durian bubble model [4]. This is a soft sphere model, describing the evolution of the spatial configuration of overlapping spheres resembling bubbles, droplets, or soft particles in a dispersed system. Even though the model is rather simple, it has been proven very useful in the research of jamming in foams and emulsions [16,17]. To further advance its capabilities to study coarsening, we have implemented interbubble gas diffusion as an additional degree of freedom to our set of dynamical equations. This is done in the spirit of Gardiner *et al.* [18], who studied coarsening in the bubble model at gas fractions far above the jamming limit. At this range the model successfully reproduced the asymptotic limit, Eq. (1), with the appropriate scaling of the average radius.

The present work represents a numerical study of coarsening in the bubble model near jamming. We present several main results. We verify and characterize the scaling state in the bubble model near jamming. Properties such as the coarsening time τ_c, exponent α, and the shape of the scale-invariant bubble size distribution, are all sensitive to the relative amplitude of gas exchange via thin films and through the continuous phase; we probe these dependencies systematically. We find that the form of the bubble size distribution at small radii shows signatures of the dominate gas exchange mechanism. Similarly, the coarsening time is nearly constant when gas exchange via the continuous phase dominates, but diverges at a critical gas fraction when gas exchange is predominantly through thin films. Finally, we show that coarsening dramatically influences mechanical response near jamming. We characterize the complex shear modulus G^* and the viscous relaxation time τ_r, both of which depend sensitively on the sample age, the coarsening time, and the gas fraction.

II. BUBBLE MODEL WITH COARSENING

We model foams using Durian's bubble model [4,19] in $D = 2$ spatial dimensions. The bubble model describes foams at the bubble level as packings of randomly distributed soft spheres (or disks in 2D) that repel elastically when they overlap. This is a reasonable approximation below jamming as well as somewhat above, where bubbles' shapes remain weakly distorted spheres. Clearly the approximation becomes unrealistic in the dry foam limit, where bubbles in real foams are polyhedra. Nevertheless, the bubble model remains well defined for arbitrary gas fraction ϕ, which is simply the ratio of the volume of all spheres to the system's volume.

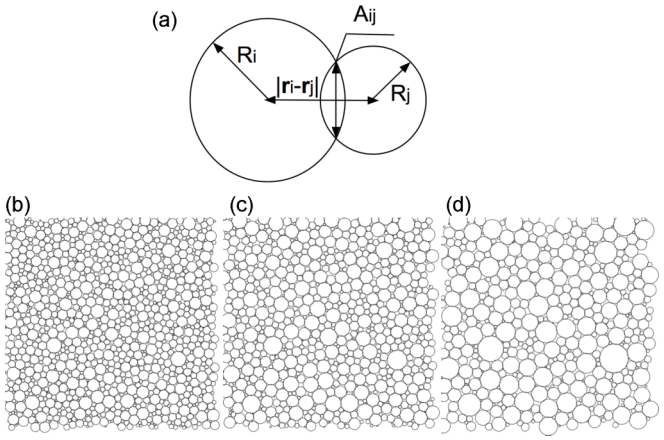

FIG. 1. (a) A schematic illustration summarizing the essential parameters of the model incorporating the interaction between two overlapping soft spheres. (b)–(d) Visualizations of a series of snapshots of the simulation: (b) shows the initial structure before coarsening, (c) is an intermediate stage, and (d) is the structure in the scaling state.

The particles in the bubble model interact via a harmonic pair potential proportional to their overlap

$$\mathbf{F}_{ij} = F_0\left(\frac{R_i + R_j - |\mathbf{r}_i - \mathbf{r}_j|}{R_i + R_j}\right)\frac{\mathbf{r}_i - \mathbf{r}_j}{|\mathbf{r}_i - \mathbf{r}_j|}, \tag{2}$$

as illustrated in Fig. 1(a). Dynamics are implemented in the fully overdamped limit: the bubbles are massless, and the force due to bubble overlap $\mathbf{F}_i$ must at all times be compensated by the drag force $\mathbf{F}_i^d = -\mu_0(\mathbf{v}_i - \langle \mathbf{v}_j \rangle)$. Here $\langle \mathbf{v}_j \rangle$ is the velocity of the background fluid often computed as the average velocity of the neighboring bubbles, and μ_0 is the viscosity of the fluid. Since we impose no external deformation to our system, we set $\langle \mathbf{v}_j \rangle = 0$. Then, the bubbles follow a quasistatic equation of motion with

$$\mathbf{v}_i = \frac{1}{\mu_0}\sum_{i \neq j}^{N} \mathbf{F}_{ij}, \tag{3}$$

which can be integrated in a molecular dynamics fashion to obtain the evolution of the foam. From considerations of dimensionality we assume that $F_0 = T_0\langle R_{\text{in}} \rangle$. In this case, the dynamics of the system is determined by ratio μ_0/T_0. Therefore, the timescale in the simulation can be chosen so that Eqs. (2) and (3) become

$$\frac{d\mathbf{x}_i}{dt} = \sum_{i \neq j}^{N} \langle R_{\text{in}} \rangle \left(\frac{R_i + R_j - |\mathbf{r}_i - \mathbf{r}_j|}{R_i + R_j}\right)\frac{\mathbf{r}_i - \mathbf{r}_j}{|\mathbf{r}_i - \mathbf{r}_j|}, \tag{4}$$

where t is dimensionless time, scaled with μ_0/T_0. The main merits of the model are that it is sufficiently simple, while it still allows us to easily vary the foam properties such as polydispersity, volume fraction, and dimensionality.

Due to the surface tension γ, there is a pressure difference Δp (the Laplace pressure) between the gas and fluid phases. In a spherical bubble the Laplace pressure $\Delta p = 2\gamma/R$ is proportional to the inverse of the bubble's radius R. Hence smaller bubbles have a higher Laplace pressure, which tends to drive gas from smaller bubbles to larger ones. To take

this into account in the bubble model, Gardiner, Dlugogorski, and Jameson (henceforth GDJ) proposed a scheme where, in addition to their elastic and viscous interactions, the bubbles are allowed to exchange gas via two distinct mechanisms [18]. The rate of change of each bubble's volume V_i ($=\pi R^2$ in 2D) is the sum of two terms,

$$\frac{dV_i}{dt} = \dot{V}_i^{\mathrm{tf}} + \dot{V}_i^{\mathrm{cp}}. \tag{5}$$

The first term $\dot{V}_i^{\mathrm{tf}}$ is the result of gas exchange through the thin film that separates two bubbles in contact. It is proportional to their contact area A_{ij} [a length of contact line in 2D, see Fig. 1(a)] and the difference in their Laplace pressures,

$$\dot{V}_i^{\mathrm{tf}} = K \sum_{j \in i} A_{ij} \left(\frac{1}{R_j} - \frac{1}{R_i} \right), \tag{6}$$

where K is the diffusion parameter, encapsulating the properties of the liquid film and the bubbles, such as the effective permeability, surface tension, and temperature. The sum runs over bubbles j in contact with i. Note that $\dot{V}_i^{\mathrm{tf}}$ tends toward zero as two bubbles lose contact. The second term in Eq. (5), $\dot{V}_i^{\mathrm{cp}}$, models gas exchange intermediated by the continuous fluid phase. This occurs in a mean fieldlike fashion,[1]

$$\dot{V}_i^{\mathrm{cp}} = 2\pi \langle R_{\mathrm{in}} \rangle \kappa (1-\phi) K \left(\frac{1}{\langle R \rangle} - \frac{1}{R_i} \right). \tag{7}$$

The dimensionless prefactor κ encodes the relative strength of liquid-intermediated diffusion versus diffusion through thin films. The proportionality with $\langle R_{\mathrm{in}} \rangle$ is introduced on dimensional grounds, while the ad hoc prefactor of $1-\phi$ imposes the reasonable requirement that no gas exchange occur via the continuous liquid phase when the liquid fraction vanishes. For the specific case of a foam monolayer sandwiched between two plates, recent calculations from Schimming and Durian [20] imply a value of κ that varies smoothly with gas volume fraction and bubble radius. Here, for simplicity and generality, we sweep ϕ at constant κ while reporting results for several values of κ.

The simulation procedure is as follows. The simulations begin by first randomly distributing the bubbles in a periodic rectangle (2D) at the initial volume fraction of $\phi = 0.45$. The initial number of bubbles varied between the simulations. The $\kappa = 0$ cases had 3000 bubbles. Our tests involving 10 000 bubbles showed no significant improvement on the data, while considerably increasing the computational cost. The computational demand was lesser for the cases where $\kappa > 0$, and all of these were run with 10 000 bubbles allowing for longer simulation times. For each bubble an initial radius is assigned according to a Gaussian distribution with the mean $\langle R_{\mathrm{in}} \rangle = 0.006$ and standard deviation $0.21 \langle R_{\mathrm{in}} \rangle$. To reach the target volume fraction ϕ_0 we then compress the structure by rescaling the dimensions of the simulation cell at a constant velocity. After the compression, we equilibrate the system by allowing the bubble positions to relax until the energy changes less than 0.0001% for 1000 iterations. This gives us an initial structure, such as the one shown in Fig. 1(b). Finally, we turn on the coarsening and run the simulations until the number of bubbles is smaller than a cutoff, which we take to be 300, and the bubble size distribution has reached the scaling state [Fig. 1(c)]. The differential equations (4)–(7) are integrated using a second-order adaptive step size predictor-corrector scheme with error tolerances set to 1×10^{-6}. In all the plots involving time, we have used the timescale $t^* = (K/\langle R_{\mathrm{in}} \rangle^2) t$. As small bubbles tend to shrink, at some point there exist bubbles with a negligibly small volume. For convenience, bubbles that shrink below a threshold 1×10^{-6} are removed, with their gas content again redistributed among the remaining bubbles in proportion to their radius and conserving ϕ.

[1]Note that Gardiner *et al.* use $\langle 1/R \rangle$ in place of $1/\langle R \rangle$ in Eq. (7). Our alteration ensures that the gas exchange summed over all bubbles is zero and the gas fraction remains invariant in time.

III. SCALING STATE

We now probe the evolution of bubble sizes as a function of time. We first identify the scaling state, and then probe how the coarsening time changes as the relative strength κ of gas diffusion through the contacts and via the continuous phase is varied.

In Fig. 2(a) we plot the average bubble size $\langle R \rangle$ as a function of time for a system with volume fraction $\phi = 0.90$ and $\kappa = 0.1$. Consistent with Eq. (1), there is an initial transient after which the observable develops a power-law dependence on time. This is the scaling state. The average bubble radius in the scaling state follows a power-law $\langle R \rangle \sim t^{*\alpha}$. By fitting this form to late-time data [Fig. 2(a)], for this particular system we find an exponent $\alpha \approx 0.425$. Due to dimensional considerations and the conservation of total volume, one expects the same exponent α to describe the growth $\langle N \rangle \sim t^{*-D\alpha}$ of the mean number of bubbles $\langle N \rangle$. This scaling relation is verified in Fig. 2(b). To further characterize the scaling state, we plot the probability density function (PDF) of bubble sizes $R/\langle R(t^*) \rangle$ in Fig. 2(c). During the transient the PDF broadens beyond the initial Gaussian distribution. In the scaling state PDF $(R/\langle R(t^*) \rangle)$ ceases to evolve with time. Hence the bubble size distribution is invariant up to an overall change in scale.

We now probe the dependence of the coarsening process on both gas fraction and the dimensionless parameter κ, which quantifies the relative strength of gas exchange through thin films and via the continuous phase. We focus on gas fractions roughly in the vicinity of the gas fraction 0.84 where jamming occurs in bidisperse disk packings [21]. In experimental systems, the value of κ can be expected to depend in a complex way on the interplay between the gas solubility, volume fraction, and the permeability of the surfactant layer. However, in contrast to experiments, in numerics it is straightforward to tune the value of κ. We therefore investigate the limit where κ is sent to zero. We are motivated by the observation that in static packings near jamming, both the mean overlap and the mean contact area between bubbles vanish as the gas fraction approaches ϕ_c from above. This suggests that gas exchange via the contacts should be strongly sensitive to the system's proximity to the jamming transition.

In Fig. 3 we plot the average radius as a function of time, with a run time of $T = 200$. We keep $\kappa = 0.1$ and vary the gas fraction from 0.82 (below jamming) to 0.95 (well above jamming). In each case the system approaches a scaling state,

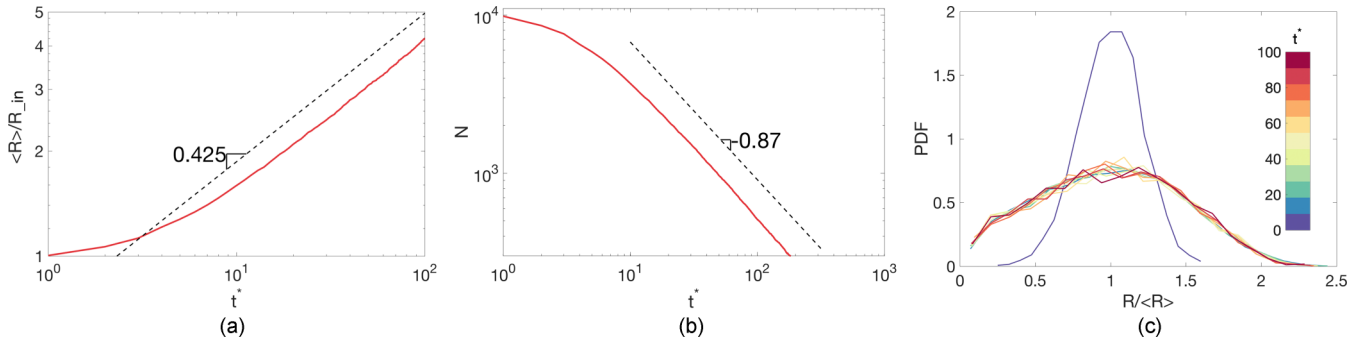

FIG. 2. (a) Time evolution of the average bubble size for gas fraction $\phi = 0.9$ and $\kappa = 0.1$ The dashed curve has a slope 0.425. (b) The number of bubbles decays in time, approaching a power law with exponent -0.87 (dashed curve). (c) The probability density function (PDF) of bubble radii R, expressed in units of the mean bubble size $\langle R(t^*)\rangle$ at time t^*. Time increases from blue to red (see legend).

but the apparent exponent α in the scaling state clearly varies. Intriguingly, power-law fits suggest $\alpha \approx 0.30$ and 0.45 for the lowest and highest values of ϕ, respectively. These are similar to the theoretical values $1/3$ and $1/2$ associated with dilute and dry foams. This observation suggests that changes in the scaling state reflect the dominant gas exchange mechanism. (The small differences between our numerical estimates of α and the theoretical predictions are likely due to finite system sizes and run times, and, for the case of large ϕ, the fact that the bubble model fails to capture the polygonal shape of bubbles in dry foam.)

In order to quantify the dependence of the scaling state on both ϕ and κ, in Fig. 4 we investigate both the exponent α and the coarsening time τ_c as a function of gas fraction ϕ for different values of κ. As shown in Fig. 4(a), the apparent α is an increasing function of ϕ for finite κ. For the special case of $\kappa = 0$ (all gas exchange occurs through thin films), the coarsening time grows dramatically (discussed below) and it becomes impractical to estimate α for $\phi < 0.9$. Above this value $\alpha \approx 0.45$.

In Fig. 4(b) we plot the coarsening time τ_c for the same data sets, estimated as the time where the average radius equals 1.5 times its initial value. In all three cases, the time required to reach the scaling state increases with decreasing ϕ. For $\kappa = 0$, the coarsening time appears to diverge. This divergence can

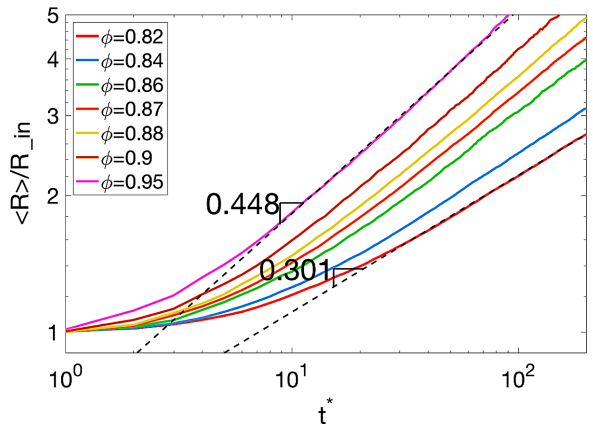

FIG. 3. Time evolution of the average bubble size for $\kappa = 0.1$ and ϕ ranging from 0.82 to 0.95.

be quantified by plotting the $\kappa = 0$ data on a log-log plot as a function of $\Delta\phi = \phi - \phi_c$ [Fig. 4(c), blue squares]. We find that for a critical gas fraction $\phi_c = 0.873$, the coarsening time is well described with a power-law $\tau_c \sim 1/\Delta\phi^\beta$ with $\beta \approx 0.8$. Estimating the coarsening time from the decay of N, rather than the average radius, gives compatible results (not shown). In the same plot, we estimate the coarsening time $\tau_c^{\rm nr}$ for *nonrattler* particles (red circles). More precisely, we calculate the average radius of load bearing particles, which are the only ones undergoing gas exchange when $\kappa = 0$. The timescale $\tau_c^{\rm nr}$ diverges more slowly; a power-law fit gives an exponent $\beta \approx 0.4$. We note that a naïve extrapolation from the bubble-bubble gas exchange law, Eq. (6), would predict a timescale that diverges as $1/A \sim 1/\Delta\phi^{0.5}$ in 2D.

Let us now summarize the results of Figs. 2–4. We observe a scaling state in the GDJ bubble model with coarsening. The effective exponent α assumes a narrow range of values 0.30–0.45 in the vicinity of the jamming transition, with a notable dependence both on ϕ and on the relative strength of gas exchange through contacts and via the continuous phase. As the ratio κ is decreased at fixed ϕ, there is a substantial increase in the the coarsening time τ_c. When κ is nonzero, the coarsening time remains finite in the vicinity of jamming, while τ_c appears to diverge at a critical volume fraction when $\kappa = 0$. The above observations lead us to hypothesize that there are two separate timescales $\tau_{\rm tf}$ and $\tau_{\rm cp}$, associated with gas exchange through thin films and via the continuous phase, respectively, and that the coarsening time τ_c is selected by the smaller of $\tau_{\rm tf}$ and $\tau_{\rm cp}$.

At gas volume fractions below jamming, nearly all the gas exchange occurs through the continuous phase, i.e., the $\dot{V}^{\rm cp}$ dominates the process. Since $\dot{V}^{\rm cp}$ depends linearly on κ, so does also the relative gas flux $\dot{V}^{\rm cp}/\dot{V}^{\rm tf}$. On the other hand when $\kappa = 0$, $\dot{V}^{\rm tf}$ is the only gas exchange mechanism available. Then, on the approach to jamming, the relative importance of $\dot{V}^{\rm tf}$ should be expected to decrease with the same power law as τ_c, $\dot{V}^{\rm tf}$ being the sole source of this scaling. The same is expected to occur also at small values of κ. At high kappa, the process is completely dominated by the $\dot{V}^{\rm cp}$ giving a scaling close to $1/3$ at all ranges of gas volume fractions.

Above we found that the coarsening time when $\kappa = 0$ diverges at a critical volume fraction $\phi_c \approx 0.873$. This value is significantly larger than the more commonly quoted value

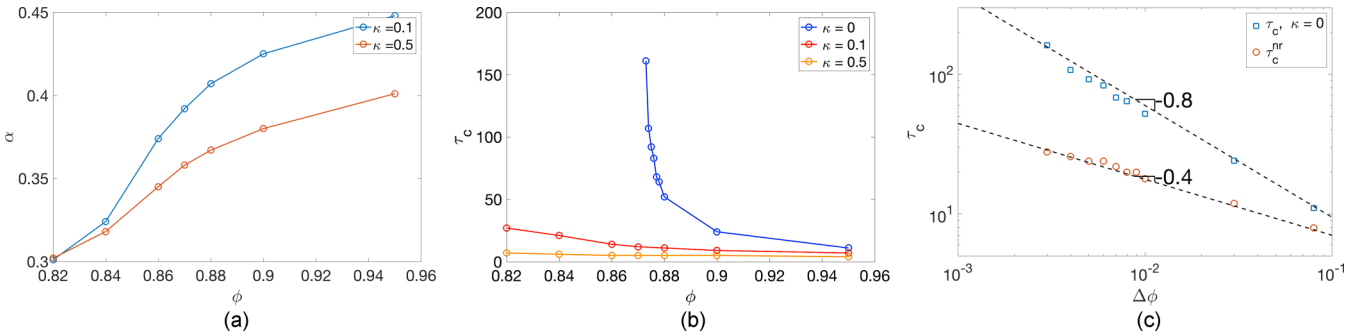

FIG. 4. (a) Power-law exponent α as a function of gas fraction ϕ for two values of $\kappa = 0.1$ and 0.5. (b) The coarsening time τ_c as a function of gas fraction ϕ for varying ratios κ (see legend). The coarsening time is defined as time when $\langle R\rangle/R_{\rm in}$ is equal to 1.5. (c) The power-law divergence of the coarsening time when $\kappa = 0$. Blue squares indicate coarsening time when all bubbles were taken into account calculating $\langle R\rangle$. Red circles indicate the coarsening time calculated when only nonrattler bubbles were considered.

around 0.842, see, e.g., Refs. [5,21,22]. As our estimation of ϕ_c was made via an indirect method, we now seek to rationalize it via independent measurements.

The critical volume fraction is known to depend on the polydispersity of a packing [21,23,24]. We therefore study the evolution of the bubble size distribution in the scaling state. In Fig. 5 we plot PDF $(R/\langle R\rangle)$ evaluated at the end of each run. The PDFs for sufficiently large κ show a gradual linear growth at small R that gives away to a broad peak near the mean bubble size. As κ decreases, the bubble size distribution broadens while simultaneously developing a large peak at small values of R corresponding to approximately 10% of the maximum bubble size. To illustrate these differences, in Figs. 5(b) and 5(c) we compare snapshots of systems with $\kappa = 0.12$ and 0 in the scaling state. In the system with $\kappa = 0$, voids between large bubbles tend to be occupied by small ones. The small bubbles are have little or no overlap with their geometric neighbors—the system on the right is effectively closer to its jamming transition, even though both systems have the same gas fraction. The void-filling bubbles of Fig. 5(c) experience little or no gas exchange until their surrounding bubbles change their configuration, which leads to the large peak in the PDF. This phenomenon survives in the scaling state because the typical size of both voids and bubbles increase in proportion to $\langle R(t^*)\rangle$. The form of the PDF may be a way to distinguish "small κ" and "large κ" systems experimentally.

The $\kappa = 0$ bubble size distribution is significantly broader than the usual bidisperse packings studied in simulations [21]. We therefore attribute the upward shift in ϕ_c to this broadening. The distinguishing feature of the present system, *vis à vis* other polydisperse systems, is that its broad bubble size distribution is not seeded via an initial condition. Instead it is dynamically generated through coarsening, and there is feedback between the evolution of the bubble size distribution and the system's proximity to the jamming transition.

To provide an independent test of the shift in ϕ_c, in Fig. 6(b) we plot the mean coordination number z for varying ϕ as a function of time. In determining z, we assume that the system's evolution is quasistatic, so that rattlers can be meaningfully identified and removed. Jamming occurs at the

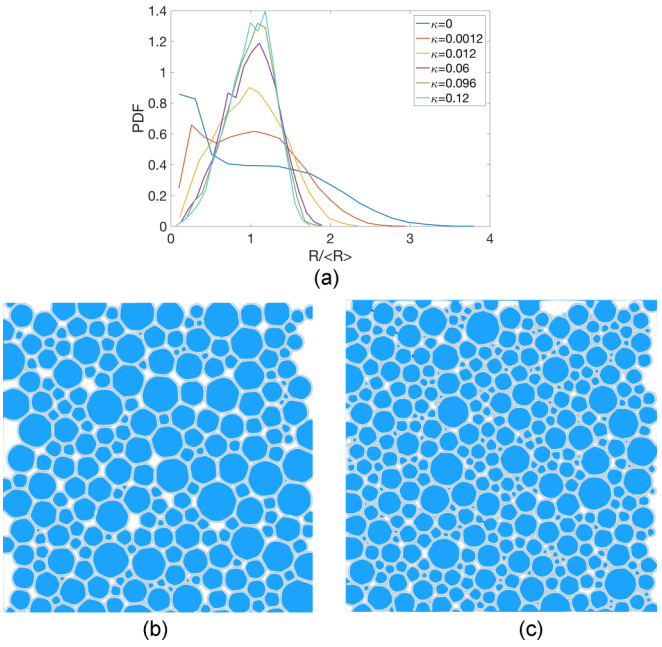

FIG. 5. (a) Probability distribution function (PDF) of the radius (normalized by $\langle R\rangle$) evaluated at $t^* = 80$ for $\phi = 0.88$ and κ ranging from 0.01 to 1.0. (b) and (c) Systems with $\kappa = 0.12$ and $\kappa = 0$ at $t^* = 100$, $\phi = 0.88$.

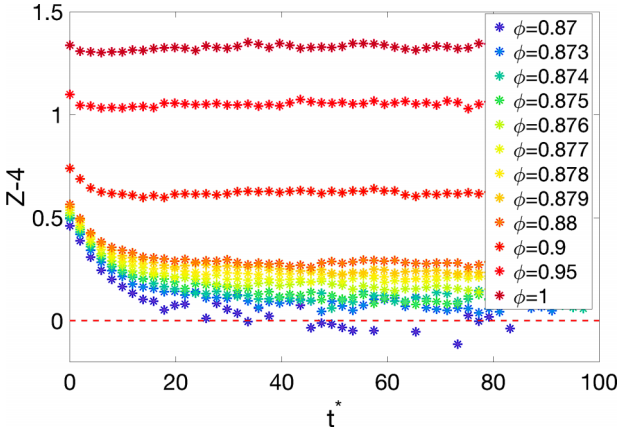

FIG. 6. Mean coordination number $z(t^*) - 4$ for varying ϕ as a function of time.

critical coordination number $z_c = 2D = 4$ in two dimensions, in accord with a constraint counting argument that dates to Maxwell. One clearly sees that packings for $\phi \geqslant 0.88$ satisfy $z > z_c$ for the entire run time, while $\phi = 0.87$ dips below 4 approximately halfway through the run—while the initial condition was jammed, the scaling state samples unjammed packings.

In order to estimate ϕ_c more accurately, we have probed the interval $0.87 \leqslant \phi \leqslant 0.88$ in steps of 0.001 for longer runs to $T = 10^3$. At these long times the system reaches sizes $N \sim O(100)$ (recall that $N \sim 1/t^{*D\alpha}$) and the coordination number experiences large fluctuations, which restricts the precision of our estimate. We find that for volume fractions $\phi \leqslant 0.872$ the mean coordination unambiguously drops below z_c within the run time, while for $\phi \geqslant 0.877$ it clearly remains above z_c. For $0.873 \leqslant \phi \leqslant 0.876$, the coordination number fluctuates on either side of z_c, so the system's evolution passes through both jammed and unjammed configurations. These observations lend independent support to the determination of ϕ_c from the divergence in τ_c presented above.

IV. MECHANICS

In the previous section we identified signatures of the jamming transition in the scaling dynamics of coarsening foams. We now seek to correlate these effects with features of the mechanical response. Our interest lies specifically with the interplay between a growing coarsening time and the foam's mechanical response. As the coarsening time actually diverges when $\kappa = 0$, we focus on this case.

Bubbles store energy when distorted and dissipate energy when sliding past each other, which gives rise to viscoelastic response [4,25]. Foam viscoelasticity can be probed both experimentally and numerically by measuring the complex shear modulus $G^*(\omega) = G'(\omega) + \imath G''(\omega)$, defined as the complex ratio of shear stress and strain amplitude under harmonic forcing at angular frequency ω [26]. The real and imaginary parts of G^* are known as the storage and loss moduli, respectively. Previous work has shown that the amplitude and shape of the complex modulus depend sensitively on the distance to the jamming transition in systems without coarsening [9,27–33].

For reference, we recall that simple viscoelastic solids (frequently referred to as Kelvin-Voigt solids) have a constant storage modulus G_0 and a linear loss modulus $\eta_0\omega$; their ratio G_0/η_0 selects a characteristic relaxation time. Deviations from the Kelvin-Voigt form are associated with a spectrum of relaxation times (rather than a single timescale), but the timescale τ_r where the loss and storage moduli cross, i.e., $G'(1/\tau_r) = G''(1/\tau_r)$, is still an important reference point. It indicates a crossover from predominantly solidlike response at low frequencies to predominantly liquidlike response at high frequencies.

While the complex shear modulus is meant to describe steady state dynamics, the structure of coarsening foams in the scaling state continuously evolves ("ages") [34,35]. Aging violates time translational invariance, which is assumed in the usual definition of the complex shear modulus [36]. Nevertheless, oscillatory rheology is often used to characterize soft materials, with a focus on frequencies that are fast compared to the evolution of the structure [34,35]. Here we determine the storage and loss moduli via a numerical "experiment" that disentangles viscous relaxation from coarsening-induced rearrangements. States are sampled at varying times t^* from a coarsening simulation at fixed ϕ. Coarsening dynamics are then turned off (all particle sizes are held fixed) and the complex shear modulus is measured according to the method described below. In this way it is possible to obtain moduli over the full range of frequencies $0 \leqslant \omega \leqslant \infty$; however, we focus on timescales that are short compared to the system's age.

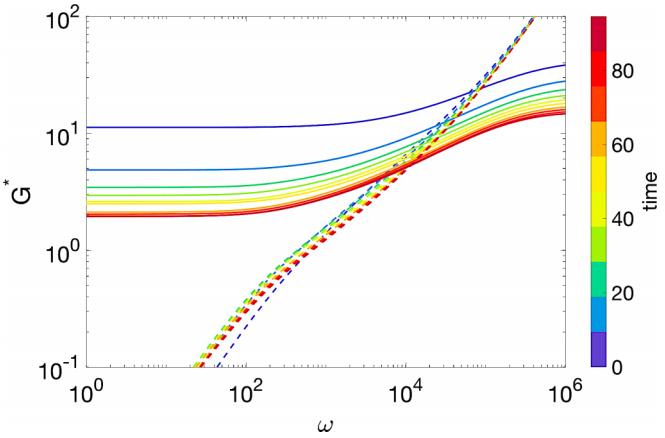

FIG. 7. Complex shear modulus G^* for $\phi = 0.878$. Solid lines depict the storage modulus G'; dashed lines depict the loss modulus G''. The color palette corresponds to evolution in time.

In order to measure the complex shear modulus, we employ a linearization scheme introduced in Ref. [9]. Given a particular configuration of bubbles, its collective response to shear is described by the $DN + 1$-component vector $\mathbf{u} = (\vec{u}_1, \vec{u}_2, \ldots, \vec{u}_D, \gamma)^T$, where $\vec{u}_i$ is the displacement of bubble i from its reference position, and γ is the shear strain experienced by the unit cell. The response to a shear stress σ is given by the solution to the first-order differential equation

$$\mathbf{K}\,\mathbf{u}(t^*) + \mathbf{B}\,\dot{\mathbf{u}}(t^*) = \sigma(t^*) V \mathbf{e}_\gamma, \tag{8}$$

where $\mathbf{e}_\gamma$ is a unit vector along the strain coordinate. The stiffness matrix $\mathbf{K}$ and damping matrix $\mathbf{B}$ describe the elastic and viscous forces on the particles, respectively. $\mathbf{K}$ consists of second derivatives of the elastic potential energy with respect to the particle and strain degrees of freedom; $\mathbf{B}$ is similarly defined in terms of the Rayleigh dissipation function. Details are available in Ref. [9]. Linearization is strictly valid only when deformation amplitudes are infinitesimal; nevertheless, numerical studies indicate that moduli calculated in this way remain accurate over a finite strain interval [30,37,38]. By Fourier-transforming Eq. (8) and solving for the complex shear strain in response to a sinusoidally oscillating shear stress with frequency ω, one can determine complex shear modulus.

In Fig. 7 we plot the storage and loss moduli (solid and dashed curves, respectively) for a system at $\phi = 0.878$, close to but above the jamming transition. The storage modulus displays a low frequency plateau, indicating that the sampled configurations are jammed solids. (We stress again that the linearization scheme employed here "turns off" coarsening,

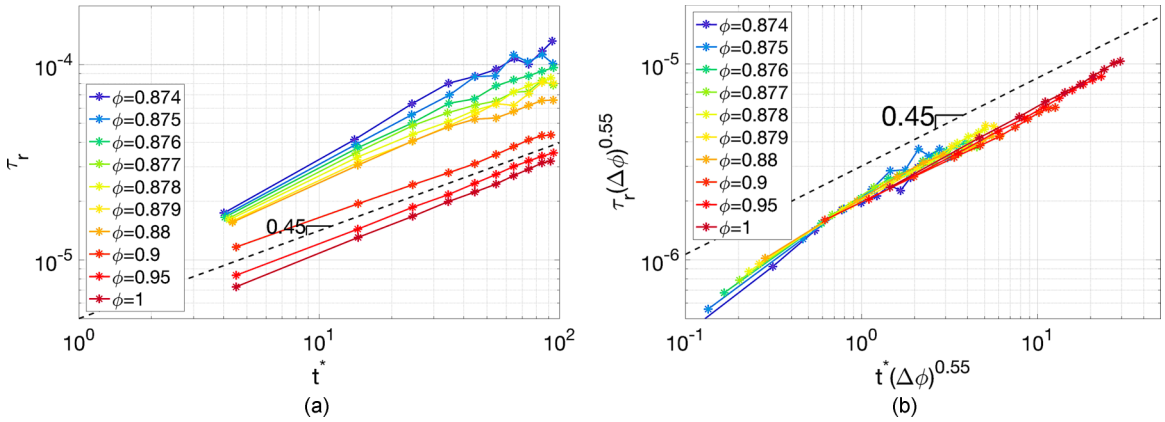

FIG. 8. (a) Mechanical relaxation time measured from the intersection of G' and G'' for different ϕ as a function of system age. (b) Data collapse: relaxation times scaled with $\Delta\phi^{0.55}$ as a function of $t^*\Delta\phi^{0.55}$.

hence any softening at asymptotically low frequencies due to coarsening-induced rearrangements will not be captured.) At high frequencies there is a second plateau in G', associated with affine deformations [9,30]. There is a gradual crossover between these two plateaus. In similar fashion, the loss modulus G'' is asymptotically linear at low and high frequencies, with a crossover between the two scaling regimes. In previous work it was shown that this crossover occupies a widening window in frequency as $\phi \to \phi_c^+$, such that $G' \sim G'' \sim \omega^{1/2}$ [9]. Experimental measurements of the loss modulus in foams often show a plateau at low frequency [34,35]. This feature is absent from our data, and from prior studies of Durian's bubble model without coarsening, including ones that probe finite strain amplitudes with rearrangements [9,30,33]. We conclude that the plateau results from physics that is not incorporated in the bubble model.

The storage modulus shows a clear dependence on the sample age, with an overall downward shift with increasing age. Their intersection point defines the mechanical relaxation time τ_r, which we measure at varying volume fraction and age—see Fig. 8(a). The relaxation time clearly depends on both the system age t^* and the distance to jamming; it grows larger with increasing age and decreasing distance to jamming $\Delta\phi$. The dependence of τ_r on t^* and $\Delta\phi$ can be rationalized in two steps, beginning with its growth with age.

The age dependence of τ_r is controlled by the scaling of G' and G'' with t^*. These can be anticipated on dimensional grounds, by which one expects there to be characteristic elastic and viscous stress scales:

$$\sigma_{\rm el} \sim \left(\frac{N(t^*)\,R(t^*)}{L^D}\right) F_{\rm el}(t^*), \tag{9}$$

$$\sigma_{\rm visc} \sim \left(\frac{N(t^*)\,R(t^*)}{L^D}\right) F_{\rm visc}(t^*). \tag{10}$$

Here N, R, $F_{\rm el}$, and $F_{\rm visc}$ are typical values of the particle number, particle radii, and elastic and viscous forces, respectively; L^D is the volume of the unit cell, which is constant. The elastic force law scales with the dimensionless overlap [cf. Eq. (2)] and should therefore be independent of time in the scaling state; hence the time dependence of the typical elastic stress scales as $\sigma_{\rm el} \sim N(t^*)R(t^*) \sim t^{*-\alpha}$. By contrast, the typical viscous force is set by the bubble velocity $V \propto R(t^*)\,\omega$. Hence $\sigma_{\rm visc} \sim t^{*0}$, consistent with observations. Turning back to τ_r, we note that the relaxation time in systems without coarsening is insensitive to the distance to jamming; hence the dependence here is likely to be inherited from the coarsening dynamics. And indeed, a simple balancing of the viscous and elastic stress scales would suggest a frequency $\omega_r \equiv 1/\tau_r$ that depends on age as $\omega_r \sim R \sim t^{*\alpha}$, consistent with the data in Fig. 8(a).

In order to understand the dependence of τ_r on $\Delta\phi$, we postulate that the nonrattler coarsening time $\tau_c^{\rm nr}$ sets the natural units for both relaxation time and the age of the system. This is expressed most naturally in the form of a scaling ansatz,

$$\frac{\tau_r}{\tau_c^{\rm nr}} \sim \mathcal{T}\left(\frac{t^*}{\tau_c^{\rm nr}}\right), \tag{11}$$

for some function $\mathcal{T}(x)$. Indeed, in Fig. 8(b) we obtain good data collapse when plotting $\tau_r\,\Delta\phi^\beta$ versus $t^*\,\Delta\phi^\beta$. Treating β as a free parameter, the best collapse is found for $\beta = 0.55$, reasonably close to the value 0.4 determined independently in Fig. 4(c) and the value 0.5 suggested by scaling analysis of Eq. (6). Comparable data collapse can be obtained using 0.5 if one restricts the gas fraction to values $\phi < 0.95$. As expected, $\mathcal{T} \sim x^\alpha$ for large values of x, when the system's age is large compared to the coarsening time τ_c. It follows that, in the scaling state, the mechanical relaxation time obeys $\tau_r \sim t^{*\alpha}/\Delta\phi^{\beta(1-\alpha)}$. Deviations from a slope of α occur when the age is smaller than the coarsening time. We expect that Eq. (11) remains valid when $\kappa > 0$, though in this case the coarsening time no longer diverges at ϕ_c.

V. CONCLUSIONS

We have presented the results of numerical simulations of the coarsening of foams close to, and slightly above, the jamming volume fraction. For this purpose, we implemented the Durian bubble model, with extensions to incorporate gas diffusion between the bubbles.

Our main observation are: (i) The model captures the expected $t^{*\alpha}$ scaling, with an exponent α whose value is sensitive to the dominant gas exchange mechanism. (ii) The

shape of the bubble size distribution signals the dominant gas exchange mechanism. When κ is large, the PDF has a broad peak near the mean bubble size; when κ is sufficiently small, a sharp peak at low R emerges. (iii) The coarsening time is also sensitive to the dominant gas exchange mechanism. When exchange is predominantly through the continuous phase, τ_c is insensitive to the gas fraction. In contrast, when gas exchange is dominated by contacts between bubbles, τ_c diverges. (iv) The foam's mechanical response is radically influenced by the coarsening; the mechanical relaxation time τ_r, where the oscillatory rheology shows a crossover from liquidlike to solidlike behavior, shows scaling both with the system's age and the nonrattler coarsening time. This establishes a clear connection between mechanical relaxation and the coarsening dynamics.

Finally, our results suggest directions for future work. In order to more deeply understand the enhanced packing efficiency of the scaling state, it would be necessary to model the form of the bubble size distribution directly. There may be fruitful connections to systems undergoing rupture and/or Apollonian packings [39,40]. Additional questions concern the dominant mechanism of gas exchange between bubbles. We expect that by appropriate choice of the gas solubility and surfactant properties, one might be able to select different values of κ in experiments. More detailed models of gas exchange could also potentially be implemented in simulations. For example, recent work has shown that there is a non-negligible flux through the plateau borders (i.e., through the packing's fluid-filled voids, rather than through the increasingly smaller thin film interfaces [20,41] close to the jamming volume fraction). This would yield additional terms in Eq. (6). Additionally, in technological applications foams often undergo shear flow during coarsening; how are these two forms of driving coupled? In addition, industrial foams are often formed of thixotropic complex fluids, such as (nano)particulate suspensions. Coarsening dynamics changes due to the nonlinear dynamics of the suspending liquid, ultimately stopping completely [41,42]—how can coarsening and mechanics be characterized and modeled in such cases? Many of these issues and questions can potentially be addressed with straightforward extensions of the present model.

ACKNOWLEDGMENTS

A.P. and K.K. are grateful to the Academy of Finland for financial support through project No. 278367 and to Aalto Science-IT project for providing access to the necessary hardware. K.B. and B.P.T. acknowledge funding from the Netherlands Organization for Scientific Research (NWO).

[1] D. L. Weaire and S. Hutzler, *The Physics of Foams* (Oxford University Press, Oxford, 2001).
[2] N. Isert, G. Maret, and C. M. Aegerter, Eur. Phys. J. E **36**, 1 (2013).
[3] F. Bolton and D. Weaire, Phys. Rev. Lett. **65**, 3449 (1990).
[4] D. J. Durian, Phys. Rev. Lett. **75**, 4780 (1995).
[5] C. S. O'Hern, L. E. Silbert, A. J. Liu, and S. R. Nagel, Phys. Rev. E **68**, 011306 (2003).
[6] P. Olsson and S. Teitel, Phys. Rev. Lett. **99**, 178001 (2007).
[7] G. Katgert, B. P. Tighe, M. E. Möbius, and M. van Hecke, Europhys. Lett. **90**, 54002 (2010).
[8] R. Lespiat, S. Cohen-Addad, and R. Höhler, Phys. Rev. Lett. **106**, 148302 (2011).
[9] B. P. Tighe, Phys. Rev. Lett. **107**, 158303 (2011).
[10] I. M. Lifshitz and V. V. Slyozov, J. Phys. Chem. Solids **19**, 35 (1961).
[11] W. Z. Ostwald, Phys. Chem. **37**, 385 (1901).
[12] D. J. Durian, D. A. Weitz, and D. J. Pine, J. Phys.: Condens. Matter **2**, SA433 (1990).
[13] J. Lambert, I. Cantat, R. Delannay, R. Mosko, P. Cloetens, J. A. Glazier, and F. Graner, Phys. Rev. Lett. **99**, 058304 (2007).
[14] J. Lambert, R. Mokso, I. Cantat, P. Cloetens, J. A. Glazier, F. Graner, and R. Delannay, Phys. Rev. Lett. **104**, 248304 (2010).
[15] I. Fortuna, G. L. Thomas, R. M. C. de Almeida, and F. Graner, Phys. Rev. Lett. **108**, 248301 (2012).
[16] A. J. Liu and S. R. Nagel, Annu. Rev. Condens. Matter Phys. **1**, 347 (2010).
[17] M. van Hecke, J. Phys.: Condens. Matter **22**, 033101 (2010).
[18] B. Gardiner, B. Dlugogorski, and G. Jameson, Philos. Mag. A **80**, 981 (2000).
[19] D. J. Durian, Phys. Rev. E **55**, 1739 (1997).
[20] C. D. Schimming and D. J. Durian, Phys. Rev. E **96**, 032805 (2017).
[21] D. J. Koeze, D. Vågberg, B. B. Tjoa, and B. P. Tighe, Europhys. Lett. **113**, 54001 (2016).
[22] K. W. Desmond and E. R. Weeks, Phys. Rev. E **80**, 051305 (2009).
[23] C. B. O'Donovan, E. I. Corwin, and M. E. Möbius, Philos. Mag. **93**, 4030 (2013).
[24] K. W. Desmond and E. R. Weeks, Phys. Rev. E **90**, 022204 (2014).
[25] R. Höhler and S. Cohen-Addad, J. Phys.: Condens. Matter **17**, R1041 (2005).
[26] H. A. Barnes and J. F. Hutton, *An Introduction to Rheology* (Elsevier, Amsterdam, 1989).
[27] T. Hatano, Phys. Rev. E **79**, 050301 (2009).
[28] B. P. Tighe, Phys. Rev. Lett. **109**, 168303 (2012).
[29] M. Otsuki and H. Hayakawa, Phys. Rev. E **90**, 042202 (2014).
[30] J. Boschan, D. Vågberg, E. Somfai, and B. P. Tighe, Soft Matter **12**, 5450 (2016).
[31] J. Boschan, S. A. Vasudevan, P. E. Boukany, E. Somfai, and B. P. Tighe, Soft Matter **13**, 6870 (2017).
[32] K. Baumgarten and B. P. Tighe, Soft Matter **13**, 8368 (2017).
[33] S. Dagois-Bohy, E. Somfai, B. P. Tighe, and M. van Hecke, Soft Matter **13**, 9036 (2017).
[34] S. Cohen-Addad, H. Hoballah, and R. Höhler, Phys. Rev. E **57**, 6897 (1998).
[35] A. D. Gopal and D. J. Durian, Phys. Rev. Lett. **91**, 188303 (2003).
[36] S. M. Fielding, P. Sollich, and M. E. Cates, J. Rheol. **44**, 323 (2000).

[37] M. S. van Deen, J. Simon, Z. Zeravcic, S. Dagois-Bohy, B. P. Tighe, and M. van Hecke, Phys. Rev. E **90**, 020202 (2014).

[38] M. S. van Deen, B. P. Tighe, and M. van Hecke, Phys. Rev. E **94**, 062905 (2016).

[39] O. Ben-Nun, I. Einav, and A. Tordesillas, Phys. Rev. Lett. **104**, 108001 (2010).

[40] S. V. Anishchik and N. N. Medvedev, Phys. Rev. Lett. **75**, 4314 (1995).

[41] S. Cohen-Addad, R. Höhler, and O. Pitois, Annu. Rev. Fluid Mech. **45**, 241 (2013).

[42] A. Britan, M. Liverts, G. Ben-Dor, S. Koehler, and N. Bennani, Colloids Surf. A **344**, 15 (2009).